

Exploiting exotic LHC datasets for long-lived new particle searches

Hesham El Faham^{a,b,c}, Andrea Giammanco^a, and Jan Hajer^d

^aCentre for Cosmology, Particle Physics and Phenomenology (CP3),
Université Catholique de Louvain, B-1348 Louvain-la-Neuve, Belgium

^bInter-University Institute for High Energies (IIHE),
Vrije Universiteit Brussel, B-1050 Brussels, Belgium

^cDepartment of Physics and Astronomy, University of Manchester,
Oxford Road, Manchester M13 9PL, United Kingdom

^dCentro de Física Teórica de Partículas (CFTP), Instituto Superior Técnico (IST),
Universidade de Lisboa, 1049-001 Lisboa, Portugal

Abstract

Motivated by the expectation that new physics may manifest itself in the form of very heavy new particles, most of the operation time of the large hadron collider (LHC) is devoted to proton-proton (pp) collisions at the highest achievable energies and collision rates. The large collision rates imply tight trigger requirements that include high thresholds on the final-state particles' transverse momenta p_T and an intrinsic background in the form of particle pileup produced by different collisions occurring during the same bunch crossing. This strategy is potentially sub-optimal for several well-motivated new physics models where new particles are not particularly heavy and can escape the online selection criteria of the multi-purpose LHC experiments due to their light mass and small coupling.

A solution may be offered by complementary datasets that are routinely collected by the LHC experiments. These include heavy ion collisions, low-pileup runs for precision physics, and the so-called 'parking' and 'scouting' datasets. While some of them are motivated by other physics goals, they all have the usage of mild p_T thresholds at the trigger-level in common. In this study, we assess the relative merits of these datasets for a representative model whose particular clean signature features long-lived resonances yielding displaced dimuon vertices. We compare the reach across those datasets for a simple analysis, simulating LHC data in Run 2 and Run 3 conditions with the DELPHES simulation. We show that the scouting and parking datasets, which afford low- p_T trigger thresholds by only using partial detector information and delaying the event reconstruction, respectively, have a reach comparable to the standard pp dataset with conventional thresholds. We also show that heavy ion and low-pileup datasets are far less competitive for this signature.

Keywords: Large Hadron Collider, Hidden sectors, Long-lived particles, Low-pileup, Scouting, Trigger-level analysis, Turbo stream, Parking, Heavy ion collisions

Contents

1	Introduction	3
2	Low scale hidden sectors	4
2.1	Benchmark model	4
3	Datasets	5
3.1	Standard pp dataset	5
3.2	Low-pileup dataset	5
3.3	Scouting dataset	6
3.4	Parking dataset	7
3.5	Heavy ion dataset	7
4	Monte Carlo simulation	9
4.1	Signal simulation	9
4.2	Background simulation	10
4.3	Detector simulation	10
5	Analysis	11
5.1	Trigger scenarios	13
6	Results and discussion	13
7	Summary and conclusion	15
A	Run 3 results	16
B	Codes and cards	16

List of Tables

1	Comparison of p_T thresholds and luminosities	8
2	Trigger scenarios	13

List of Figures

1	Feynman diagram of the benchmark process	9
2	Dimuon invariant mass distributions	11
3	Transverse impact parameter distributions	12
4	Run 2 significances: Datasets	14
5	Run 2 significances: Triggers scenarios	15
6	Comparison of significances	16
7	Run 3 significances: Datasets	17
8	Run 3 significances: Triggers scenarios	18

1 Introduction

Since the inception of the large hadron collider (LHC), the experiments at its ring have collected a tremendous amount of data and utilised them to search for hints of physics beyond the standard model (BSM). Most of the run time at the LHC and the data stored by its main experiments are dedicated to high-energy proton-proton (pp) collisions. However, a fraction of time and storage are also devoted to special datasets motivated by specific physics goals. Examples include heavy ion runs (nucleus-nucleus or proton-nucleus collisions), motivated by the study of the quark-gluon plasma and other high-energy nuclear physics phenomena, and low-luminosity pp runs designed to provide clean events for precise measurements of some standard model (SM) parameters for which no large amounts of data are necessary.

Any dataset, regardless of its nature, is filtered by *triggers*, i.e. sets of selection criteria that are applied online, based on partial detector information in order to provide a sufficiently rapid decision, since storing all collision events is impossible for a hadron collider such as the LHC. Both ATLAS and CMS can store events on tape at a maximum rate of the order of one thousand events per second, shared across a large number of trigger paths. Therefore, the bandwidth allocated to each trigger is limited, with a larger bandwidth allocated to the triggers that give more sensitivity to the studies assigned higher priority by the collaborations that operate the experiments.

As the LHC luminosity increases, there are two basic strategies at the trigger-level to cope with the increased collision rate within a fixed bandwidth: tightening the selection criteria and, in particular, the p_T thresholds, or keeping the same thresholds but recording only a subset of the events that would otherwise pass the trigger selection. The latter strategy is called *prescaling*. The former strategy is traditionally favoured in BSM searches, based on the expectation that any new particles would be massive and therefore decay into very high p_T final-state particles or generate a large transverse momentum imbalance E_T^{miss} when particles remain undetected. Such expectation is supported by the most popular models of new physics, such as supersymmetry, extra dimensions, and gauge unification models.

Trigger thresholds of LHC experiments are carefully optimised such that the primary stored pp dataset is sensitive to as many new physics signals as possible. However, it has been suggested that new physics could be generated in collisions at the LHC but is then disregarded by the trigger requirements; see e.g. [1–3] and references therein. This is especially true for BSM models that predict *soft* decays, i.e. which do not lead to events with large p_T particles or large E_T^{miss} . Examples include axion-like particles (ALPs), heavy neutral lepton (HNL), or new gauge bosons, each with masses of an order of a few GeV [4–8]. While the authors of reference [8] argue for new ways of triggering for the standard dataset, we further argue that some existing triggers have sufficiently low thresholds in some non-standard datasets. Thus, we explore whether enhancing the resources allocated to those *exotic* datasets might be convenient in future runs and whether or not they can be promising in this respect.

This article reports a comparative study of the prospects to constrain this kind of BSM physics using the standard pp collisions with large pileup, a low-pileup pp sample, heavy ion collisions, and pp collisions saved with the scouting and parking approaches. We rely on simulated data where the DELPHES fast detector simulation [9] is used to emulate the detector effects corresponding to a generic LHC multi-purpose detector in Run 2 and Run 3 conditions.

This article is organised as follows. Section 2 presents a specific category of BSM signals, predicted in so-called *hidden sector* models, which are notoriously difficult to detect by the multi-purpose LHC experiments, and elaborates on a particular signature (displaced dimuons) that is found in several of those models and is experimentally clean. The alternative datasets

collected by LHC experiments are described in section 3. Section 4 provides details on the simulation of signal and background events under the conditions corresponding to the various datasets considered. Section 5 describes a simple data-analysis strategy for identifying the benchmark signature, whose results are presented in section 6. Finally, we summarise the lessons learned in section 7. The predictions for the sensitivities achievable during Run 3 are collected in appendix A and the code used for the generation of signal and backgrounds is given in appendix B.

2 Low scale hidden sectors

Many models predict new feebly interacting light degrees of freedom, such as ALPs, HNLs, and additional gauge bosons, potentially as messengers to an extensive hidden sector [10, 11]. Despite their small masses, they can have evaded detection until now due to their small couplings, which can induce tiny production cross sections and unusual long lifetimes. However, they might appear in high-luminosity experiments or dedicated low-energy collider datasets. Therefore, the exotic datasets considered here present an exciting opportunity to search for manifestations of such models. For this study, we use a benchmark model with a scalar particle and adjust its coupling such that it is long-lived and therefore decays in a secondary vertex. While the coupling strength in this specific simplified model is not particularly well-motivated on its own, the signature of a displaced decay with soft tracks generated by this simple model is a common prediction of more complicated models and a worthwhile target for dedicated searches. Therefore, we treat this simplified benchmark model as a proxy for a class of BSM models featuring such a signature.

2.1 Benchmark model

Additional particles with spin zero can solve significant problems in particle physics, such as the strong CP problem of quantum chromodynamics (QCD). One famous example is the axion originating in the spontaneous breaking of the anomalous global $U(1)$ Peccei–Quinn symmetry [12]. The associated (pseudo) Nambu-Goldstone boson (PNGB) has a fixed relation between coupling strength, mass, and the symmetry-breaking scale. However, here we consider more generic pseudoscalar particles, generally called ALPs, which are not subject to this restriction.

Effective field theories (EFTs) provide a model-independent approach to parameterising the effects of potential new physics in low-energy data [11]. One example is the Standard Model effective field theory (SMEFT) [13] built in terms of towers of operators constructed out of the SM fields and respecting the SM symmetries, ordered by their mass dimension. It is possible to add the interactions of generic PNGBs to the SMEFT [11]. The resulting model has been published in the form of the FEYNRULES [14] model file ALPSEFT [15]. The part of the ALPs EFT Lagrangian relevant to this study is

$$\mathcal{L}_a = \frac{1}{2} \partial_\mu a \partial^\mu a - \frac{1}{2} m_a a^2 - c_{\tilde{G}} \frac{a}{f_a} G_{\mu\nu} \tilde{G}^{\mu\nu} - i c_{a\phi} \frac{a}{f_a} \sum_f m_f (\bar{f}_L f_R - \text{h.c.}) + \dots, \quad (1)$$

where a is the ALPs field with mass m_a and decay constant f_a . The coefficients of the coupling with the gluon field strength tensor $G_{\mu\nu}$ and its dual $\tilde{G}^{\mu\nu} \equiv \epsilon^{\mu\nu\rho\sigma} G_{\rho\sigma}/2$ is $c_{\tilde{G}}$ (**CGtil**) while after electroweak symmetry breaking its coupling to fermions f with mass m_f is $c_{a\phi}$ (**CaPhi**). In simple models the decay constant f_a is generically much larger than the electroweak scale. However, in ALPs models, it suffices to adjust it such that this new physics scale is beyond the reach of current experiments $f_a \sim \mathcal{O}(\text{TeV})$. The values of the couplings in the vicinity of the parameter space we are interested in is constrained by prior experiments. For example for low ALP masses, i.e. $m_a \lesssim 60 \text{ MeV}$, a limit of order $4c_{\tilde{G}}/f_a \lesssim 10^{-5} \text{ GeV}^{-1}$ have been set on the

ALP-gluon coupling at 90 % confidence level (CL) [15] and for masses of $1 \text{ MeV} \lesssim m_a \lesssim 3 \text{ GeV}$ limits on the ALP-fermion interaction has been set at the order of $|c_{a\phi}|/f_a < (10^{-8}\text{--}10^{-6}) \text{ GeV}^{-1}$ at 90 % CL [15].

3 Datasets

In the following, we introduce the LHC datasets compared in this study. We present the actual conditions for those datasets during the LHC Run 2, which took place between 2015 and 2018, and those that can be realistically expected for the next few years during the recently started Run 3 (2022–2025). For the latter, it is important to stress that the resources allocated to non-standard datasets, meaning the running time, the bandwidth, and the data volume, depend on decisions based on the community consensus regarding the scientific priorities of the experiments and negotiations between several analysis teams. Consequently, for Run 3, any estimate of the future amount of events is essentially an educated guess. Therefore, the predictions of this study for future datasets are presented in a form that is easily scalable to different amounts of data.

3.1 Standard pp dataset

During most of the LHC running time, the aim is to maximise the delivered instantaneous luminosity. The proton beams cross every 25 ns, and several pp collisions occur during the same bunch crossing, leading to the *pileup* of several uncorrelated collisions into a single recorded event. This results in a nuisance for the measurements, as it obfuscates the interpretation of the events, particularly the kinematic reconstruction of decay chains.

During Run 2, the two multi-purpose experiments ATLAS and CMS accumulated 140 fb^{-1} at a center of mass (CM) energy of $\sqrt{s} = 13 \text{ TeV}$ each, with an average pileup of about 35 interactions per recorded event. However, with large differences in the pileup profile between different data-taking periods [16, 17]. Typical muon selection thresholds are around 24 and 17 GeV for single-muon and dimuon triggers, respectively, see e.g. [18, 19]. The goal for the recently-started Run 3 is to accumulate about twice that amount of data at the slightly larger collision energy of $\sqrt{s} = 13.6 \text{ TeV}$. Various accelerator parameters will be tuned towards that end. One of the side effects will be an increase in the average pileup, which will roughly double with respect to Run 2. Although considerably lower than the very high pileup conditions expected during the runs of the high luminosity phase of the large hadron collider (HL-LHC) [20], i.e. from Run 4 onward, such increase of the average pileup in Run 3 may lead to a slight degradation of the performances of the particle identification and reconstruction algorithms of the experiments. One example is that it may affect the discriminating power of lepton isolation and the identification of displaced vertices.

For simplicity, we approximated the pileup profile of Run 2 by generating the corresponding Monte Carlo (MC) sample with a mean of 35 pileup interactions per event at $\sqrt{s} = 13 \text{ TeV}$. Similarly, to emulate Run 3 data, we generated a MC sample with a mean of 70 interactions per event at $\sqrt{s} = 13.6 \text{ TeV}$.

3.2 Low-pileup dataset

For a minimal time during every run, the LHC is operated on purpose at very low instantaneous luminosity to ensure low-pileup conditions. Such an experimentally clean dataset can be optimally exploited for measurements that are not limited by statistical uncertainty but are critically affected by detector systematics. An example of this measurement is the determination of the W

boson mass, a critical input to any SM consistency check. In the context of our study, which is related to long-lived particles (LLPs), the absence of pileup brings the specific advantage of ideal identification of the primary interaction vertex and precise reconstruction of secondary vertices.

The Run 2 low-pileup dataset at $\sqrt{s} = 13$ TeV mostly consists of about 0.2 fb^{-1} collected in a few days at the end of 2017, with an average pileup of two collisions per bunch crossing [21]. Given the negligible degradation of detector performances at such a low pileup, we approximate these conditions by simulating a dataset without any pileup. Additional 0.3 fb^{-1} of low-pileup data were collected at $\sqrt{s} = 5.02$ TeV in 2015 and 2017, primarily to serve as reference data for heavy ion studies but are not considered here. In this study, we assume a muon p_T thresholds of 17 and 8 GeV for single-muon and dimuon triggers, respectively, as applied by CMS in the low-pileup runs of 2017 [21].

It is not easy to foresee the amount of low-pileup data that the multi-purpose experiments will be willing to accumulate in Run 3. The priority for this kind of data may have risen after the recent publication of the legacy CDF measurement of the W mass [22], in tension with previous measurements and therefore urgently demanding updates from the LHC experiments. In this study, we assume 0.5 fb^{-1} in Run 3, i.e. the same amount of low-pileup data as during the entire Run 2 but wholly at high energy, which, in this case, means $\sqrt{s} = 13.6$ TeV. This assumption is arbitrary and shall be understood as merely representing an order of magnitude estimate.

3.3 Scouting dataset

The concept of ‘scouting’ was introduced by the CMS experiment in Run 1 [23–26]. After a pilot scouting run in 2011, it has been operated regularly since 2012 in CMS. During Run 2, it has also been used by ATLAS [27, 28] (where it is called ‘trigger-level analysis’) and LHCb [29] (where it is known as ‘turbo stream’).

Scouting is based on assigning a fraction of the bandwidth to a stream of data with reduced event content. The name comes from the possibility of *scouting* those data very early for the presence of striking signs of new physics (e.g. narrow resonances) that do not require the full power of a holistic offline analysis to be identified and that would otherwise be filtered away by the tight standard triggers. Scouting events are acquired in parallel with standard pp data. Therefore, they share the same accelerator conditions, particularly the amount of pileup. Only a minimal amount of high-level information from the online reconstruction is stored for the selected events. This implies that the reconstruction of the physics objects is less precise in this dataset than in the standard pp one, as the online reconstruction algorithms are optimised more for speed than for resolution or other performance metrics. However, this strategy permits a more significant fraction of events to be stored and analysed, allowing, in particular, looser trigger thresholds.

The LHC experiments have used the scouting data to search for dijet [27, 30] and dimuon [31] resonances, as well as LLPs [32]. Similarly to the scouting-based search reported in reference [31], this study is based on a two-muon final state signature; therefore, we assume the same Run 2 integrated luminosity as utilised in that publication. Although the CMS scouting stream was taking data during the entire Run 2, a high-rate dimuon trigger appropriate for the type of analysis studied in this paper was employed only in 2017 and 2018, with a dimuon p_T threshold of 3 GeV, accumulating 96.6 fb^{-1} [26].

For Run 3, CMS reverts to the original scouting design entirely based on particle-flow objects, increases the bandwidth, and makes the data format more offline-like. In our study, instead of doubling the Run 2 dataset as assumed for the standard pp dataset, we assume a factor of three increase. This accounts for the following factors:

- The dimuon trigger appropriate for this final state was not applied in all sub-periods of

Run 2, while it is likely to be used from start to end in Run 3 and future data acquisitions.

- Since scouting is now a more established concept whose usefulness is more broadly appreciated than just a few years ago, larger bandwidth is now allocated to it.

However, such an increase of usable scouting data from Run 2 to Run 3 is, to a large extent, an educated guess, as the bandwidth allocated to scouting is a tuneable parameter to be fixed according to community priorities.

3.4 Parking dataset

The ‘parking’ concept consists in storing a fraction of the triggered data without running the prompt reconstruction algorithms. The event reconstruction is delayed to later periods without data taking; when the experiments’ computing resources are not used at full capacity. The CMS experiment applied this concept for the first time with about twelve billion events collected in 2018, of which roughly ten billion are estimated to contain b -quarks [33], which were processed after the end of Run 2. This dataset was specifically called ‘ b -parking’ because it was motivated by b -physics goals and therefore designed such that it mostly contained events with b -quarks, with a set of triggers that included most notably a non-isolated single-muon path with a p_T threshold of 12 GeV. In principle, parking can be optimised for other physics studies and additional trigger paths with the same underlying approach of loosening the selection with respect to the standard LHC dataset are being considered.

In this study, we work with a simplified definition of a b -parking dataset, which assumes that all the events are collected through a single-muon path with displacement but without requiring the muons to be isolated, meaning they do not have to be separated from other particles in the same event.

The number of events to be collected by parking during Run 3 is potentially much larger compared to Run 2, but difficult to foresee as it depends on future available computing resources and priorities within the LHC experiments. For Run 3, we scale the number of events by a factor of four, assuming that for every year of running, it will be possible to park as many events as in the b -parking dataset of 2018.

Since resources are saturated at the start of a LHC fill when the instantaneous luminosity and hence the pileup is most significant, events start to be parked only when the instantaneous luminosity falls below a specific value. Therefore, pileup is, in principle, milder in the parking dataset than in the standard pp one. This effect is challenging to model reliably, so for simplicity, in this study, we conservatively assume that the average pileup is identical to the standard pp dataset.

3.5 Heavy ion dataset

Besides the standard pp collision, the LHC experiments collect heavy ion data. While primarily collected in PbPb collisions, heavy ion data can also be gathered from p Pb ones. Moreover, some amount of OO and p O data are scheduled for Run 3, and several other options are being discussed for the HL-LHC [34, 35]. Typically one month of every year is allocated to heavy ion operations, compared to six or seven months for pp collisions in a typical LHC year. The primary purpose of these special runs is to accumulate a deeper understanding of the quark-gluon plasma known to have permeated the early universe. Related topics in high-energy nuclear physics are also addressed with the same data. Furthermore, it has been recently realised that the heavy ion dataset constitutes a suitable environment for a few new physics searches, for which analyses based on these data can outperform the pp collisions-based ones [36, 37]. For example, searches for magnetic monopoles [38–41] and ALPs [42–44] have been carried out. It has also been

Dataset	p_T^{\min}/GeV		$\mathcal{L}_{\text{int}}/\text{fb}^{-1}$		MC approximation
	muon	dimuon	Run 2	Run 3	
Standard pp	24	17	140	280	Pileup of 35 and 70
Low-pileup	17	8	0.2	0.5	Zero pileup
Scouting	–	3	96.6	289.8	Pileup of 35 and 70
Parking	12	–	48.8	195.2	Pileup of 35 and 70
Heavy ion	–	3	1.6×10^{-6}	9.6×10^{-6}	Only PbPb

Table 1: Comparison of the p_T thresholds of the single muon and dimuon triggers simulated in this study, together with the integrated luminosities collected during the LHC Run 2 and the integrated luminosity expected after Run 3 for all datasets considered in this paper. Note that the integrated luminosity of the parking dataset is estimated from the number of events collected by CMS in Run 2 after the comparison with the b -quark cross section calculated using PYTHIA.

proposed to search for LLPs in heavy ion collisions [6, 45], as well as in electron-ion ones [46]. Additionally, attention has been given to the searches for dark photons [47], strangelets [48, 49], and sphalerons [50], also to studying $g - 2$ of the τ -lepton [51, 52].

Thanks to the relatively low event rate, dimuon events can be selected at the trigger level without any explicit p_T threshold (see e.g. [53, 54]), which roughly corresponds to an implicit threshold of 3 GeV arising from the maximum track curvature that permits it to cross the detector.

The main limitation of the heavy ion datasets is that their maximum instantaneous luminosity is orders of magnitude lower than that of pp collisions. This is due to the disruptive electromagnetic effects that depend on large powers of the atomic number Z and therefore penalise heavy ion collisions much more than light ones. This is discussed at length e.g. in [36], while the LLP search proposed in [6, 45] scans over several nuclear species to identify the most optimal one taking those effects into account. Moreover, the maximum achievable CM energy per nucleon is smaller than that of the standard pp operations since the acceleration depends on Z while the inertia depends on the mass number A . The CM energy per nucleon has been 5.02 TeV for PbPb collisions during Run 2. At the time of writing, the LHC experiments discuss the CM energy to be used in Run 3, particularly whether keeping the same CM energy as during Run 2 or taking data at higher energy. The theoretical maximum that the LHC can potentially reach is 5.5 TeV.

Two advantages of heavy ion data partially compensate for these limitations. The multiplicity of partonic interactions scales approximately as A^2 , which in the case of $^{208}_{82}\text{Pb}$ beams implies a factor of $\sim 4 \times 10^4$ enhancement,¹ and the triggers are much looser because of the low instantaneous luminosity. Moreover, heavy ion collisions provide a low-pileup environment, yet the track multiplicity is much higher than in individual pp collisions. This difference in track multiplicity is largely compensated when pp collisions include $\mathcal{O}(100)$ pileup interactions per event, as calculated in [45]. The large track multiplicity does not dramatically affect the analysis performance for clean final states with muons. In contrast, vertex multiplicity is essential if the signal muons are predicted to be displaced.

The multi-purpose experiments at the LHC collected $1.6 \times 10^{-6} \text{ fb}^{-1}$ of PbPb data during Run 2. Plans for LHC ion operation in Run 3 foresee to reach $9.6 \times 10^{-6} \text{ fb}^{-1}$ [55]. For this study, we do not consider the impact of data collected during the collisions of other ions.

¹The enhancement is even more spectacular for processes initiated by $\gamma\gamma$ interactions, as in that case, the cross sections scale as Z^4 . This effect has been exploited in the searches presented in [41, 43, 44].

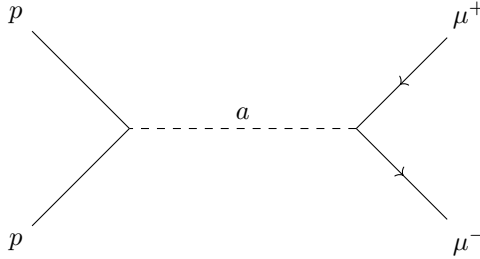


Figure 1: Feynman diagram of the pp initialised ALPs signal process introduced in section 2.1. The ALP constitutes a simple example for the light, feebly interacting, and long-lived new particle signatures considered in this paper.

For the datasets presented in this section, table 1 summarises the lowest threshold for the single-muon and dimuon triggers together with the integrated luminosity collected during Run 2 and the one assumed for Run 3. Furthermore, we give the main approximation we have applied while simulating these datasets.

4 Monte Carlo simulation

In sections 4.1 and 4.2, we present the details of the MC simulations of the signal and background events, respectively, for all the datasets. Subsequently, we discuss the simulation of the detector effects in section 4.3. All adjustments to the cards are collected in appendix B.

4.1 Signal simulation

The signal events are generated using the FEYNRULES [14] model file ALPsEFT [15]. The signal process consists of an ALP in the s -channel decaying to two muons as shown by the Feynman diagram in figure 1 and is generated using MADGRAPH5_AMC@NLO 3.10 [56]. The incoming b -quarks are chosen to be massless and included in the parton distribution functions (PDFs) through the use of the five flavour scheme (5FS). The Wilson coefficients of the operators that modify the interaction of the ALPs to fermions and gluons are chosen to be $c_{\tilde{G}} = c_{a\phi} = 10^{-5}$ while the other coefficients of the model are set to zero. The small effective coupling ensures the ALPs are long-lived and thus displaced. The partial width of the ALP into its different decay channels is calculated automatically by MADGRAPH and we do not impose any generation-level cuts.

Proton collisions The pp collisions are simulated at a CM energy of $\sqrt{s} = 13 \text{ TeV}$ and $\sqrt{s} = 13.6 \text{ TeV}$ for Run 2 and Run 3 samples, respectively, using the PDF N° 230000 from the LHAPDF [57] set containing the NNPDF 2.3 next-to-leading order (NLO) global fit with $\alpha_s(m_Z) = 0.119$ [58].

Heavy ion The heavy ion collisions are simulated at a CM energy of $\sqrt{s} = 5.02 \text{ TeV}$ and $\sqrt{s} = 5.5 \text{ TeV}$ for Run 2 and Run 3 samples, respectively, using the PDF N° 901300 from the LHAPDF set encoding the EPPS16 nuclear PDF based on the CT14 proton PDF at NLO with running α_s for $^{208}_{82}\text{Pb}$ [59, 60]. Since MADGRAPH simulates the cross section for a single nucleon the resulting cross section has to be scaled up by a factor of e.g. 208^2 in the case of lead.

4.2 Background simulation

Background events are simulated using PYTHIA 8.245 [61] by generating b -jets via QCD in gg and $q\bar{q}$ initial-states above a minimum p_T threshold of 20 GeV. This phase-space corresponds to a p_T requirement on the generated B -mesons. We only consider background events that contain at least one b -quark and one anti- b -quark with final state muons. The background generation is further optimised by imposing additional generation-level cuts:

- An upper limit on the vertex radius of the dimuon system of $r_v < 2.5$ mm
- A minimum threshold on the muons' transverse momenta of $p_T(\mu) > 2$ GeV
- A lower limit on the invariant mass of the dimuon system of $m_{\mu\mu} > 0.5$ GeV
- The muons' transverse impact parameter is required to be greater than $|d_0^\mu| > 0.5$ mm

The last cut reflects that we are primarily interested in a background environment characterised by low- p_T and high displacement and is inspired by the selection of [62], which was optimised for the even harsher pileup conditions expected for the HL-LHC.

Parking For the parking dataset, we generate $gg/q\bar{q} \rightarrow b\bar{b}$ events in PYTHIA. We apply the requirement of having at least one muon or anti-muon per generated event. The events are then passed through our analysis code which removes $\sim 50\%$ of the generated events. Therefore, the cross section obtained from PYTHIA is scaled accordingly. The calculated cross section can be used to translate the number of events into an equivalent integrated luminosity, and we obtain that the 10^9 b -parking events stored during Run 2 [26] correspond to an equivalent luminosity of 48.8fb^{-1} , see also table 1.

Heavy ion For the heavy ion background simulation, we use the ANGANTYR model integrated into PYTHIA [63]. Extrapolating the dynamics of pp collisions to the ones of nuclei, this model builds up the complete hadronic final states in high energy nuclear collisions.

4.3 Detector simulation

The LHC detector effects are simulated with DELPHES 3.4.2 [9] using a modified DELPHES card, based on a standard CMS card provided with the software package.² For the purpose of this study, the differences between the ATLAS and CMS detectors are not considered essential. Therefore, we generalise our conclusions to both multi-purpose LHC detectors. DELPHES allows to simulate the effect of pileup, and the user can control the emulation of necessary detector nuisances such as inefficiencies, misidentification, and loss of precision, which are adapted to the different scenarios considered in this comparative study.

Pileup The pileup events are added to the hard events during the detector simulation in DELPHES using the built-in pileup card that utilises PYTHIA's ability to generate soft QCD events. Except for some rare SM processes, these events are designed to represent the total cross section at a hadron collider. Out of a reservoir of 5×10^4 minimum bias events³, we add for each hard event an average of 35 pileup events for Run 2 simulations and 70 pileup events for Run 3 simulations.

² The DELPHES cards define the parameters of the detector simulation.

³ Minimum bias events are defined experimentally as the most inclusive data the experiment can trigger on. In DELPHES, they are defined by a set of PYTHIA generator cards that comprise inelastic pp collisions with a large cross section [64, 65].

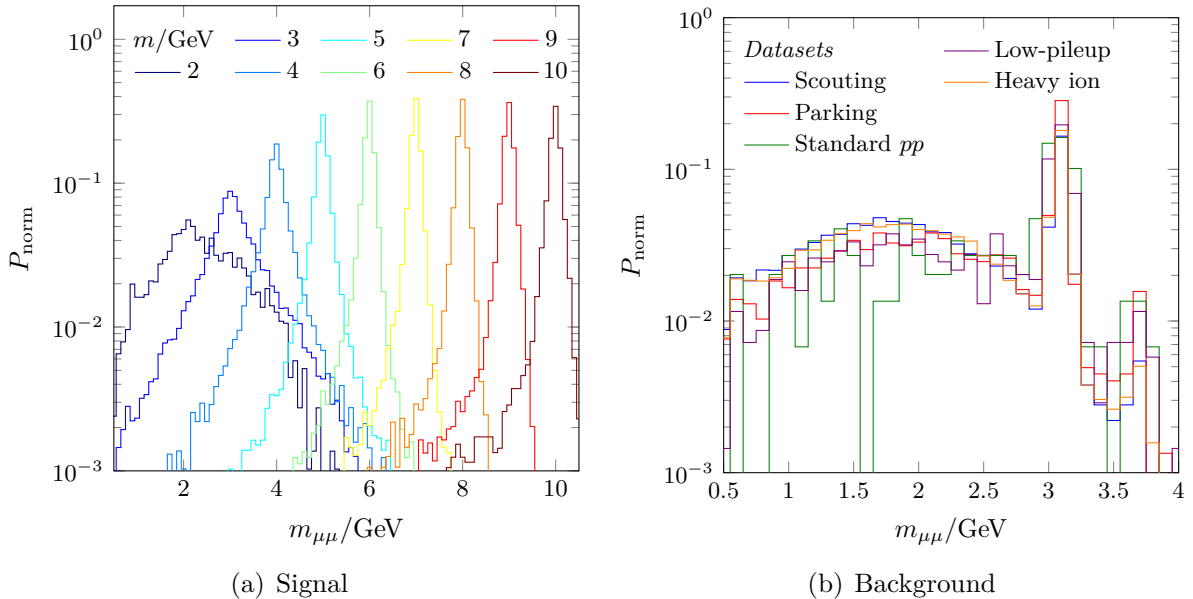


Figure 2: Probability distribution function P_{norm} as function of the dimuon invariant mass for the signal events with nine different masses in panel (a) and the background events for the five different datasets in panel (b). The signal distributions are shown for the scouting dataset. The hybrid trigger thresholds are used for both the signal and background distributions.

Scouting As discussed in section 3, the quality of event reconstruction in the scouting dataset is reduced compared to the usual pp runs. Therefore, for the simulation of the scouting data, we have degraded the momentum resolution of muons according to the formula given in appendix B, which is inspired by the degradation observed in CMS scouting data with dimuon events [31]. In that CMS study, the degradation in $m_{\mu\mu}$ resolution depended significantly on the p_T and the $|\eta|$ of the two muons. The p_T resolution of muons with $p_T < 50$ GeV is 1% in the central barrel region of the detector, defined by $|\eta| < 0.9$, and 3% in the end caps of the muon system, defined by $|\eta| > 1.2$. A smooth interpolation between 1 and 3% has been implemented in our simulation. A cut of $|\eta| < 1.9$ was applied in reference [31] because higher $|\eta|$ values lead to a much less pure sample of muon candidates, and there is not enough information at the scouting level to be able to clean the dataset. Consequently, we apply the same cut in our analysis. Although those details are taken from a CMS publication, we assume that similar constraints would be motivated in any LHC analysis. Finally, we also impose a threshold of $p_T > 3$ GeV on the analysis level to account for the geometrical acceptance of the detector, which is discussed in detail in section 5.

Parking For the parking dataset, we use the track smearing module of DELPHES to calculate the error on the track impact parameter. The latter is used in defining the impact parameter significance (IPS), which is utilised in the parking analysis, as mentioned below.

5 Analysis

The baseline output of DELPHES allows identifying only the primary vertex of a given event. Since we are primarily interested in long-lived topologies and displaced vertices, we have implemented a vertexing algorithm for reconstructing the dimuon system arising from the LLPs decay. In this vertexing algorithm, we only take as input the tracks identified as muon candidates by the

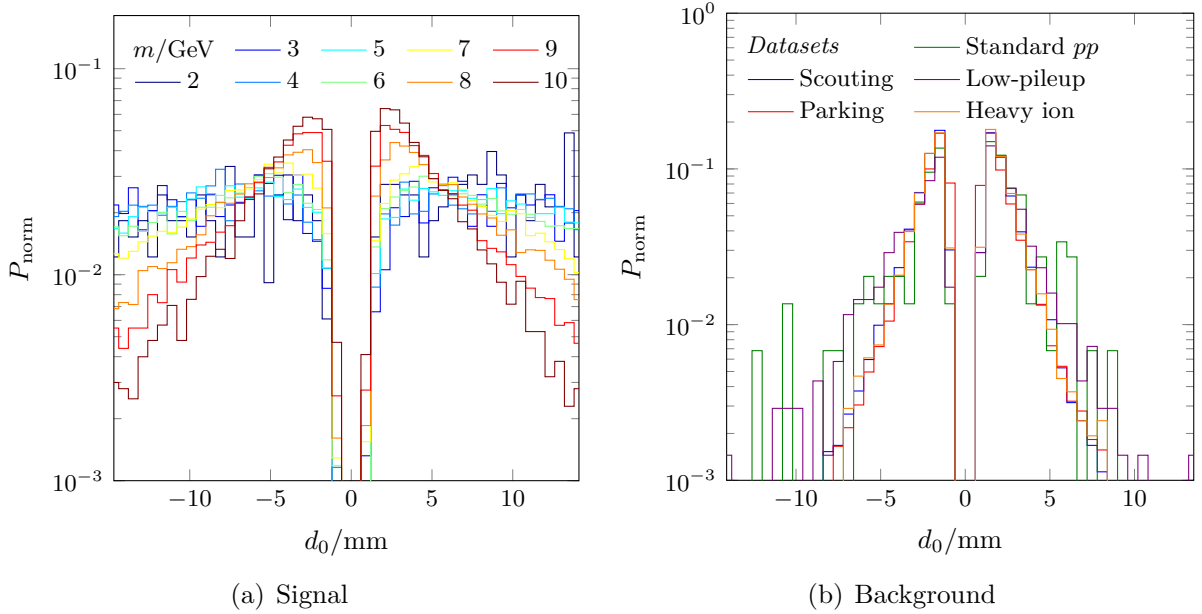


Figure 3: Probability distribution function P_{norm} as function of the transverse impact parameter of the signal events for nine different mass points in panel (a) and the background events for the five different datasets in panel (b). The signal distributions are shown for the scouting dataset. The hybrid trigger thresholds are used for both the signal and background distributions.

dedicated identification module in DELPHES, which includes both an emulation of inefficiencies as well as fakes. Our algorithm first identifies potential dimuon system candidates and then proceeds by imposing the p_T trigger thresholds collected in table 1. A further refinement is attained by tightening the selection cuts used in the background simulation to $r_v < 2 \text{ mm}$ and $|d_0^\mu| > 1 \text{ mm}$. Additional requirements are needed to simulate the scouting and the parking datasets.

Scouting Given that higher values of the pseudorapidity $|\eta|$ lead to much fewer clean muon candidates, rejecting forward candidates is necessary for a clean reconstruction of the dimuon system as mentioned in section 4.3. We, therefore, impose a cut of $|\eta_\mu| < 1.9$ on both muon tracks as in reference [31].

Parking For the simulation of the parking sample, and in line with the CMS level-1 muon trigger logic [33], we impose a similar requirement, namely a cut of $|\eta_\mu| < 1.5$ on at least one muon candidate. In order to further improve the trigger purity, at least one muon candidate is required to pass the lower threshold in the track IPS, i.e. $|d_0/d_0^{\text{err}}| > 6$ [33], where d_0^{err} is the error associated to the d_0 measurement and calculated by DELPHES.

During the analysis the two muon tracks of the dimuon system are sorted according to their displacement in terms of the transverse impact parameter $|d_0^\mu|$. The dimuon candidate that has the highest displaced track is selected. Our interest in topologies with highly displaced muon tracks motivated the analysis strategy.⁴

⁴ We have checked that the number of events with more than one dimuon candidate is negligible and have therefore not specified which potential dimuon candidate must be taken in such a case.

	Muon	Hybrid	Dimuon
p_T threshold	Single muon		Dimuon
Number of displaced muons	1		2

Table 2: Summary of the three trigger scenarios used in this analysis. The single muon and dimuon p_T thresholds for each of the datasets are given in table 1.

5.1 Trigger scenarios

The analysis was performed for three trigger scenarios: the single muon, dimuon, and hybrid trigger scenario. The single muon and hybrid trigger scenarios are characterised by the requirement of having a single muon candidate passing the single muon p_T threshold. The difference between these triggers is that the single muon trigger requires only one muon to pass the displacement cut on the transverse impact parameter, i.e. $|d_0| > 1$ mm. In contrast, the hybrid trigger imposes this requirement on both muon candidates. The dimuon trigger scenario requires both muon candidates to pass the dimuon p_T threshold and the displacement cut mentioned above. The two trigger thresholds for the different datasets are collected in table 1, and the three trigger scenarios are summarised in table 2.

We conclude this section by presenting the signal distributions for the mass of the dimuon system and the track impact parameter in nine different mass points in the scouting dataset using the hybrid trigger thresholds in figures 2a and 3a, respectively. These plots serve as an assessment of our vertexing algorithm’s efficiency. The background distributions for the same two observables for all the datasets and using the hybrid trigger thresholds are given in figures 2b and 3b. In the background distributions, aligning with our expectation, the ‘onia’ peak is apparent at around 3 GeV, corresponding to the J/ψ meson resonances.

6 Results and discussion

Since we do not intend to investigate a particular new physics model but rather comment on the comparative potentials to discover new physics signals across the different datasets collected at the LHC, we refrain from giving an absolute unit for the significance. The relevant information encoded in our results is the relative strength for discovering a displaced low- p_T signature compared between the different datasets and trigger scenarios.

The signal significance is defined as $Z = s/\sqrt{s+b}$, where s and b are the numbers of signal and background events predicted in the dimuon mass window, respectively. The width of the dimuon mass window is, in all cases, $\pm 40\%$ around the invariant mass $m_{\mu\mu}$ under consideration. The predicted number of signal and background events are obtained by using scale factors f ,

$$s = s_{\text{MC}} f_s, \quad b = b_{\text{MC}} f_b, \quad (2)$$

where s_{MC} and b_{MC} are the number of signal and background events counted in the corresponding MC samples that fall within the dimuon mass window. The f_s and f_b scale factors are defined by the luminosity ratios $\mathcal{L}_{\text{data}}/\mathcal{L}_{\text{MC}}$. The MC luminosity is obtained by normalising the number of generated MC events to the process cross section. For example, $\mathcal{L}_{\text{MC}}^{\text{bkg}} = N_{\text{gen}}^{\text{bkg}}/\sigma_{\text{bkg}}$ where $N_{\text{gen}}^{\text{bkg}}$ was chosen in our case to be 5×10^5 of generated MC background events and σ_{bkg} is the cross section calculated by PYTHIA. The luminosity of the data is the fixed integrated luminosity,

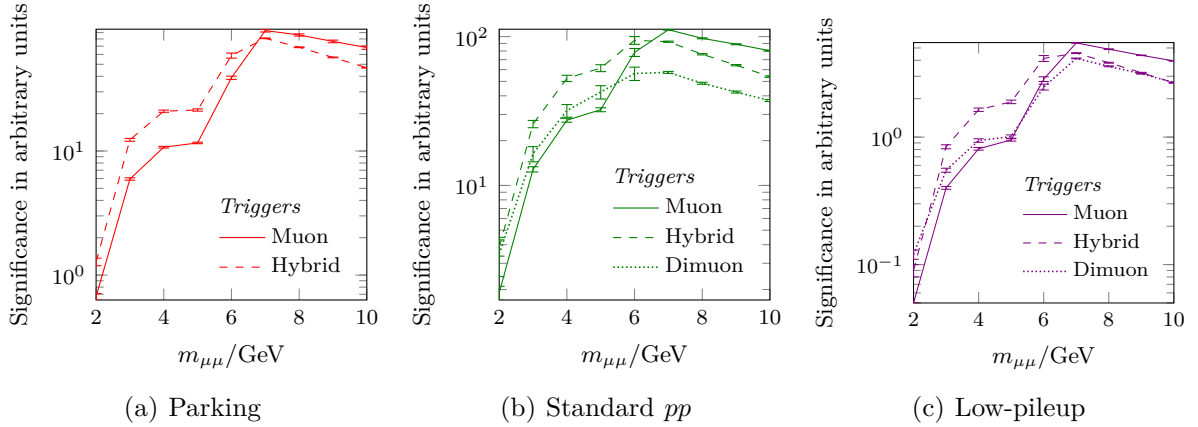


Figure 4: Comparison of the significance to discover the displaced low- p_T signal in arbitrary units as a function of the dimuon invariant mass. The comparison is shown for three of the five datasets: parking (a), standard pp (b), and low-pileup (c) for the three different triggers scenarios during Run 2. Since only the dimuon trigger applies to the scouting and heavy ion dataset, we omit these datasets here.

$\mathcal{L}_{\text{data}}$, and is given in table 1 for each type of dataset. Although negligible, the error of the quantity Z due to the size of the MC samples is propagated and reported in the plots using,

$$(\delta Z)^2 = (\partial_s Z \delta s)^2 + (\partial_b Z \delta b)^2 = \frac{s}{4} \frac{(2b + s)^2 f_s + b s f_b}{(b + s)^3} \quad (3)$$

where the uncertainties on the number of signal δs and background δb events are taken to be the Poisson distributed errors $\sqrt{s_{\text{MC}}}$ and $\sqrt{b_{\text{MC}}}$, respectively.

We present the comparison between the relevant trigger scenarios for three of the five datasets for Run 2 in figure 4. We omit the scouting and heavy ion datasets since only the dimuon trigger scenario applies to these datasets. The results for Run 3 are given separately in figure 7 of appendix A.

For $m_{\mu\mu} \geq 7 \text{ GeV}$ the single muon trigger scenario leads to the highest significance, followed by the hybrid trigger scenario. This renders the dimuon trigger scenario the least competitive for these masses. For signals with a large invariant mass $m_{\mu\mu}$, our observation suggests the importance of the high p_T threshold that the single muon and hybrid trigger scenarios impose on the muon candidates in comparison to the dimuon trigger scenario. On the other hand, for $m_{\mu\mu} \leq 6 \text{ GeV}$ the hybrid trigger scenario proves the most competitive favouring the combination of the high p_T threshold along the displacement of *both* muon tracks.

At this point, it is worth reminding that both the single muon and the hybrid trigger scenarios impose the same p_T threshold on the muon candidates. Nevertheless, the former requires one displaced muon track, while the latter requires the displacement of both tracks. This remark suggests why the hybrid trigger scenario is favoured over the single muon trigger scenario in the low-mass regions. The resonance decay in the low-mass region is long-lived and induces a high displacement of both tracks. In comparison, the decays in the high-mass region are prompter. Requiring the displacement of both muon tracks in the high-mass region induces a loss of statistics arising from discarding those events in which both tracks are produced promptly.

Having discussed the roles of the different trigger scenarios in reconstructing the dimuon signal, we now present figure 5 to compare the potential of each dataset in accessing such signal. It is clear from figure 5 that the low-pileup and heavy ion datasets demonstrate the least competition

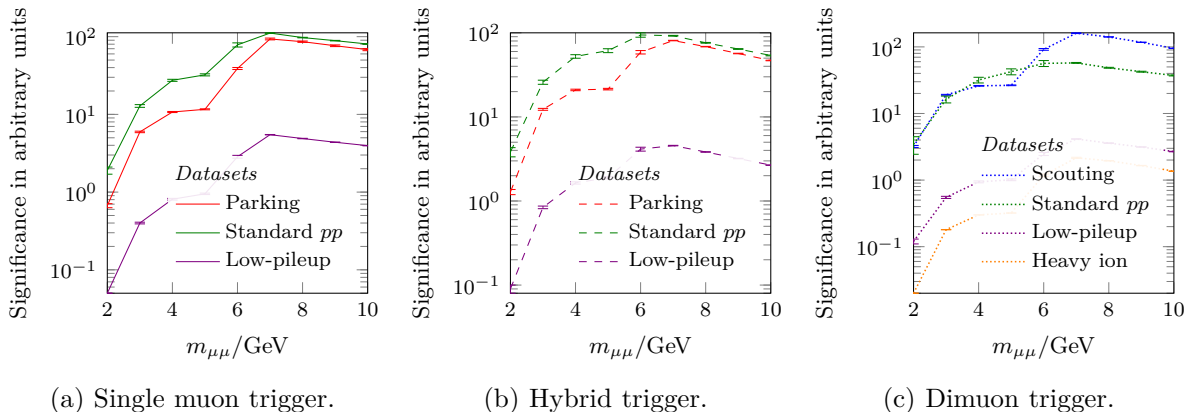


Figure 5: Comparison of the significance to discover the displaced low- p_T signal in arbitrary units as a function of the dimuon invariant mass. The comparison between the relevant datasets is shown for the single muon (a), hybrid (b), and dimuon (c) trigger scenarios during Run 2.

in accessing the dimuon signal. This is indeed expected due to the small amount of collected data compared to the other three datasets. For the dimuon trigger scenario, the scouting dataset partially outperforms the conventional LHC pp dataset. We attribute this dominance of the scouting dataset to the privileged low- p_T thresholds of the scouting triggers along the large amount of collected data. Additionally, the parking dataset is competitive with the standard pp dataset in the high-mass region.

We conclude this section by summarising in figure 6 all the LHC Run 2 results presented in figures 4 and 5 together with the complete overview of the Run 3 results. A detailed presentation of the Run 3 results is given in appendix A. Here we remark that the different expected scaling for the Run 3 luminosities enables the scouting and parking datasets to outperform the standard pp datasets in the high-mass region.

7 Summary and conclusion

We have compared different types of datasets collected at the LHC experiments using a simple model featuring a displaced vertex signature. We have shown that the scouting and parking datasets can be competitive with the standard LHC runs for such signatures in the mass region under consideration. In contrast, the low-pileup and heavy ion datasets are limited to considerably smaller significance.

We stress that although these results have been obtained for one particular signature of a specific model, its general conclusions may be generalised to some extent. We caution the reader that many assumptions have been made in this study and that DELPHES is not meant to be an accurate detector simulation. Therefore, some subtleties ignored in this paper may alter the relative ranking of some of the datasets considered. However, our results indicate that scouting and parking can be very promising strategies for a large category of signals characterised by low particle masses. Therefore, it may be worth allocating significantly larger bandwidth for those datasets than in previous runs.

Acknowledgments

First of all, we thank Marco Drewes for contributing to the initial idea of this paper and critically accompanying its development. Furthermore, we thank Olivier Mattelaer for the original implementation and continuous support for heavy ion collision simulation in MADGRAPH. Pavel

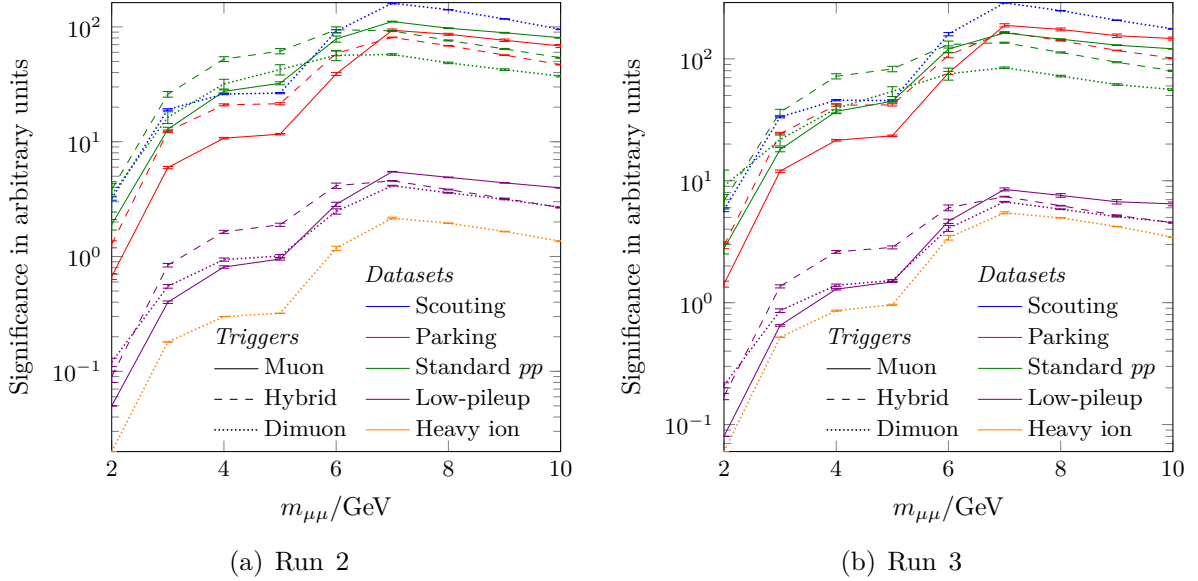


Figure 6: Comparison of the significance to discover the displaced low- p_T signal in arbitrary units as a function of the dimuon invariant mass. The comparison between the relevant datasets and trigger scenarios for Run 2 and Run 3 are shown in panels (a) and (b), respectively.

Demin and Michele Selvaggi’s assistance with the DELPHES software was pivotal in completing this project. Thanks to Christian Bierlich for discussions concerning PYTHIA, particularly on using the ANGANTYR model. We are grateful for our early talks with Simon Knapen, Steven Lowette, and Hardik Routray. HF thanks Ken Mimasu for the technical discussions on the ALPSEFT model. We received essential clarifications about scouting and parking in CMS from Greg Landsberg and Maurizio Pierini. Finally, we thank the IT team of CP3 for their assistance with the supercomputing facilities.

HF was supported by the Fond de la Recherche Scientifique de Belgique (F.R.S.-FNRS) under the excellence of science (EOS) be.h project N° 30820817. The work of JH was partially supported by Portuguese Fundação para a Ciência e a Tecnologia (FCT) through the projects CFTP-FCT Unit UIDB/00777/2020 and UIDP/00777/2020. Computational resources have been provided by the supercomputing facilities of the Université catholique de Louvain (CISM/UCL) and the Consortium des Équipements de Calcul Intensif en Fédération Wallonie Bruxelles (CÉCI) funded by the F.R.S.-FNRS under convention 2.5020.11 and by the Walloon Region.

A Run 3 results

This section presents the results for Run 3 of the LHC. In figure 7, we show the comparison between the trigger scenarios for each of the datasets; in figure 8, we show the comparison between the datasets for each of the trigger scenarios. The corresponding integrated luminosities of the different types of datasets are given in table 1.

B Codes and cards

This section presents the code used to generate the events used in this analysis.

Signal The ALP signal presented in figure 1 is generated in the s -channel and decayed to two muons using MADGRAPH

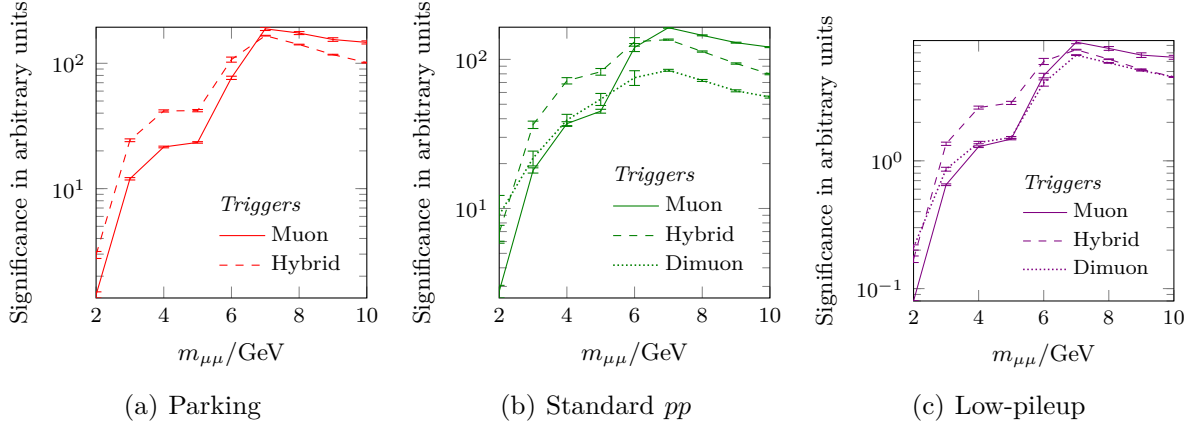


Figure 7: Comparison of the significance to discover the displaced low- p_T signal in arbitrary units as a function of the dimuon invariant mass. The comparison is shown for three of the five datasets: parking (a), standard pp (b), and low-pileup (c) for the three different triggers scenarios during Run 3. Since only the dimuon trigger applies to the scouting and heavy ion dataset, we omit these datasets here.

```
define p = g u c d s b u~ c~ d~ s~ b~
p p > ax > mu+ mu-
set mb 0
set ymb 0
```

In order to use the 5FS the mass of the bottom quark and its coupling are set to be zero. The ALPSEFT [15] model is adjusted by changing the `param.card` values

```
CGtil = CaPhi = 0.00001
```

We ensure that all time of flight information are stored in the Les Houches event files by adjusting the `run.card` using

```
time_of_flight = 0.0mm
```

The PDF for the pp datasets is included via

```
nn23lo1:230000
```

while the PDF of the PbPb dataset is included via

```
lhpdf:901300
```

Background For the background simulation PYTHIA is generally initialised with

```
HardQCD:gg2bbbar
HardQCD:qqbar2bbbar
PhaseSpace:p_ThatMin = 20
```

For the pp simulations we use the default conditions, i.e.

```
Beams:idA = 2212
Beams:idB = 2212
Beams:eCM = 13600.0 # Run 3
Beams:frameType = 1
```

and for the heavy ion background simulation we use

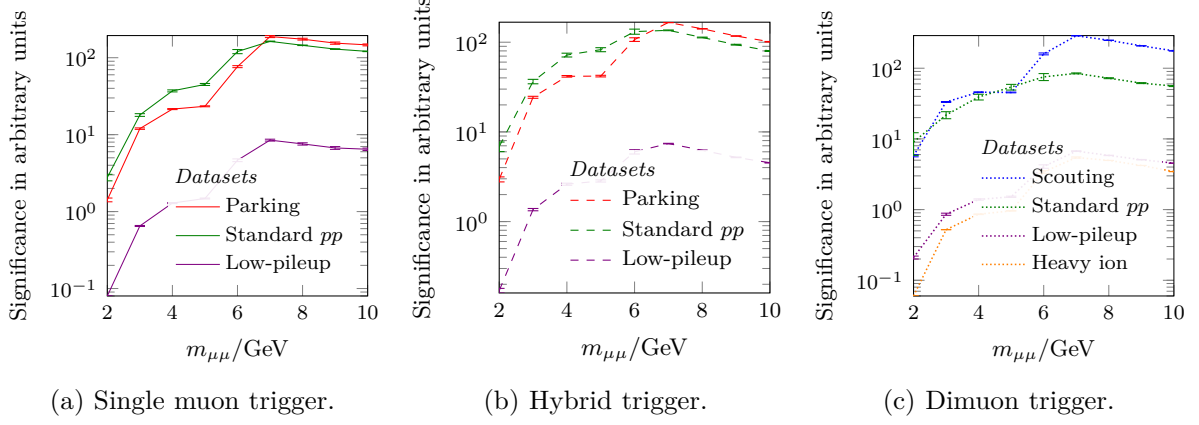


Figure 8: Comparison of the significance to discover the displaced low- p_T signal in arbitrary units as a function of the dimuon invariant mass. The comparison between the relevant datasets is shown for the single muon (a), hybrid (b), and dimuon (c) trigger scenarios during Run 3.

```
Beams:idA = 1000822080
Beams:idB = 1000822080
Beams:eCM = 5500.0 # Run 3
HeavyIon:mode = 1
```

The pileup events are generated using the DELPHES `minbias` generation card which utilise the `SoftQCD` switch of PYTHIA

Detector For the scouting dataset, the muon tracking resolution is degraded in the DELPHES CMS card using

```
set ResolutionFormula{
  (abs(eta) <= 0.9) * (pt > 0.1 && pt < 50) * (0.01) +
  (abs(eta) > 0.9 && abs(eta) <= 1.2) * (pt > 0.1 && pt < 50) *
    (0.01 + (abs(eta) - 0.9) * 0.01 * (2/3)) +
  (abs(eta) > 1.2 && abs(eta) <= 1.9) * (pt > 0.1 && pt < 50) * (0.03) +
  (abs(eta) <= 0.5) * (pt > 50) * sqrt(0.01^2 + pt^2 * 1.0e-4^2) +
  (abs(eta) > 0.5 && abs(eta) <= 1.5) * (pt > 50) *
    sqrt(0.015^2 + pt^2 * 1.5e-4^2) +
  (abs(eta) > 1.5 && abs(eta) <= 2.5) * (pt > 50) *
    sqrt(0.025^2 + pt^2 * 3.5e-4^2)
}
```

corresponding to the arguments made in reference [31].

References

- [1] J. Alimena et al. ‘Searching for long-lived particles beyond the Standard Model at the Large Hadron Collider’. In: *J. Phys. G* 47.9 (2020), p. 090501. DOI: 10.1088/1361-6471/ab4574. arXiv: 1903.04497 [hep-ex].
- [2] M. Borsato et al. ‘Unleashing the full power of LHCb to probe stealth new physics’. In: *Rept. Prog. Phys.* 85.2 (2022), p. 024201. DOI: 10.1088/1361-6633/ac4649. arXiv: 2105.12668 [hep-ph]. №: FERMILAB-PUB-21-343-T.

- [3] O. Fischer et al. ‘Unveiling hidden physics at the LHC’. In: *Eur. Phys. J. C* 82.8 (2022), p. 665. DOI: 10.1140/epjc/s10052-022-10541-4. arXiv: 2109.06065 [hep-ph].
- [4] M. J. Strassler. ‘Possible effects of a hidden valley on supersymmetric phenomenology’ (July 2006). arXiv: hep-ph/0607160.
- [5] M. J. Strassler and K. M. Zurek. ‘Echoes of a hidden valley at hadron colliders’. In: *Phys. Lett. B* 651 (2007), pp. 374–379. DOI: 10.1016/j.physletb.2007.06.055. arXiv: hep-ph/0604261.
- [6] M. Drewes, A. Giammanco, J. Hajer, M. Lucente, and O. Mattelaer. ‘Searching for New Long Lived Particles in Heavy Ion Collisions at the LHC’. In: *Phys. Rev. Lett.* 124.8 (2020), p. 81801. DOI: 10.1103/PhysRevLett.124.081801. arXiv: 1810.09400 [hep-ph]. №: CP3-18-60.
- [7] M. Drewes and J. Hajer. ‘Heavy Neutrinos in displaced vertex searches at the LHC and HL-LHC’. In: *JHEP* 02 (2020), p. 070. DOI: 10.1007/JHEP02(2020)070. arXiv: 1903.06100 [hep-ph]. №: CP3-19-11.
- [8] F. Blekman, N. Desai, A. Filimonova, A. R. Sahasransu, and S. Westhoff. ‘Soft displaced leptons at the LHC’. In: *JHEP* 11 (2020), p. 112. DOI: 10.1007/JHEP11(2020)112. arXiv: 2007.03708 [hep-ph]. №: TIFR/TH/20-21 and P3H-20-029.
- [9] J. de Favereau, C. Delaere, P. Demin, A. Giammanco, V. Lemaître, A. Mertens, and M. Selvaggi. ‘DELPHES 3: A modular framework for fast simulation of a generic collider experiment’. In: *JHEP* 02 (2014), p. 057. DOI: 10.1007/JHEP02(2014)057. arXiv: 1307.6346 [hep-ex]. Code: *Delphes: A framework for fast simulation of a generic collider experiment*. Mar. 2009. DOI: 10.5281/zenodo.821635. GitHub: delphes/delphes. URL: cp3.irmp.ucl.ac.be/projects/delphes.
- [10] P. Agrawal et al. ‘Feebly-interacting particles: FIPs 2020 workshop report’. In: *Eur. Phys. J. C* 81.11 (2021), p. 1015. DOI: 10.1140/epjc/s10052-021-09703-7. arXiv: 2102.12143 [hep-ph].
- [11] C. Arina, J. Hajer, and P. Klose. ‘Portal Effective Theories. A framework for the model independent description of light hidden sector interactions’. In: *JHEP* 09 (2021), p. 063. DOI: 10.1007/JHEP09(2021)063. arXiv: 2105.06477 [hep-ph].
- [12] R. D. Peccei and H. R. Quinn. ‘CP Conservation in the Presence of Instantons’. In: *Phys. Rev. Lett.* 38 (1977), pp. 1440–1443. DOI: 10.1103/PhysRevLett.38.1440. №: ITP-568-STANFORD.
- [13] I. Brivio and M. Trott. ‘The Standard Model as an Effective Field Theory’. In: *Phys. Rept.* 793 (2019), pp. 1–98. DOI: 10.1016/j.physrep.2018.11.002. arXiv: 1706.08945 [hep-ph].
- [14] A. Alloul, N. D. Christensen, C. Degrande, C. Duhr, and B. Fuks. ‘FeynRules 2.0: A complete toolbox for tree-level phenomenology’. In: *Comput. Phys. Commun.* 185 (2014), pp. 2250–2300. DOI: 10.1016/j.cpc.2014.04.012. arXiv: 1310.1921 [hep-ph]. №: CERN-PH-TH-2013-239, MCNET-13-14, IPPP-13-71, DCPT-13-142, and PITT-PACC-1308. Code: *FeynRules: A Mathematica package to calculate Feynman rules*. June 2008. URL: feynrules.irmp.ucl.ac.be.
- [15] I. Brivio, M. B. Gavela, L. Merlo, K. Mimasu, J. M. No, R. del Rey, and V. Sanz. ‘ALPs Effective Field Theory and Collider Signatures’. In: *Eur. Phys. J. C* 77.8 (2017), p. 572. DOI: 10.1140/epjc/s10052-017-5111-3. arXiv: 1701.05379 [hep-ph]. №: IFT-UAM-CSIC-16-141, KCL-PH-TH-2016-72, FTUAM-16-49, and CP3-17-04. Code: *ALPsEFT: Effective Theories for a light Axion-Light-Particle (ALP)*. FeynRules model file. 2017. URL: feynrules.irmp.ucl.ac.be/wiki/ALPsEFT.

- [16] *CMS. Luminosity: Public results.* URL: twiki.cern.ch/twiki/bin/view/CMSPublic/LumiPublicResults.
- [17] *ATLAS. Luminosity: Public results Run 2.* URL: twiki.cern.ch/twiki/bin/view/AtlasPublic/LuminosityPublicResultsRun2.
- [18] *ATLAS.* ‘Searches for new phenomena in events with two leptons, jets, and missing transverse momentum in 139 fb^{-1} of $\sqrt{s} = 13\text{ TeV}$ pp collisions with the ATLAS detector’ (Apr. 2022). arXiv: 2204.13072 [hep-ex]. №: CERN-EP-2022-014.
- [19] *CMS.* ‘Search for CP violation in $t\bar{t}H$ and tH production in multilepton channels in proton-proton collisions at $\sqrt{s} = 13\text{ TeV}$ ’ (Aug. 2022). arXiv: 2208.02686 [hep-ex]. №: CMS-HIG-21-006 and CERN-EP-2022-157.
- [20] X. Cid Vidal et al. ‘Report from Working Group 3: Beyond the Standard Model physics at the HL-LHC and HE-LHC’. *Report on the Physics at the HL-LHC, and Perspectives for the HE-LHC*. Ed. by A. Dainese, M. Mangano, A. B. Meyer, A. Nisati, G. Salam, and M. A. Vesterinen. Vol. 7. Dec. 2019, pp. 585–865. DOI: 10.23731/CYRM-2019-007.585. arXiv: 1812.07831 [hep-ph]. №: CERN-LPCC-2018-05.
- [21] *CMS.* ‘Measurement of the inclusive $t\bar{t}$ production cross section in proton-proton collisions at $\sqrt{s} = 5.02\text{ TeV}$ ’. In: *JHEP* 04 (2022), p. 144. DOI: 10.1007/JHEP04(2022)144. arXiv: 2112.09114 [hep-ex]. №: CMS-TOP-20-004 and CERN-EP-2021-244.
- [22] *CDF.* ‘High-precision measurement of the W boson mass with the CDF II detector’. In: *Science* 376.6589 (2022), pp. 170–176. DOI: 10.1126/science.abk1781. №: FERMILAB-PUB-22-254-PPD.
- [23] D. Anderson. ‘Data Scouting in CMS’. In: *PoS ICHEP 2016* (2016), p. 190. DOI: 10.22323/1.282.0190. №: CMS-CR-2016-339.
- [24] J. Duarte. ‘Fast Reconstruction and Data Scouting’. *4th International Workshop Connecting The Dots 2018*. Aug. 2018. arXiv: 1808.00902 [hep-ex]. №: FERMILAB-CONF-18-370-CMS-E-PPD.
- [25] G. Badaro et al. ‘40 MHz Level-1 Trigger Scouting for CMS’. In: *EPJ Web Conf.* 245 (2020). Ed. by C. Doglioni, D. Kim, G. A. Stewart, L. Silvestris, P. Jackson, and W. Kamleh, p. 01032. DOI: 10.1051/epjconf/202024501032.
- [26] S. Mukherjee. ‘Data Scouting and Data Parking with the CMS High level Trigger’. In: *PoS EPS-HEP2019* (2020), p. 139. DOI: 10.22323/1.364.0139.
- [27] *ATLAS.* ‘Search for low-mass dijet resonances using trigger-level jets with the ATLAS detector in pp collisions at $\sqrt{s} = 13\text{ TeV}$ ’. In: *Phys. Rev. Lett.* 121.8 (2018), p. 081801. DOI: 10.1103/PhysRevLett.121.081801. arXiv: 1804.03496 [hep-ex]. №: CERN-EP-2018-033.
- [28] *ATLAS.* ‘Performance of electron and photon triggers in ATLAS during LHC Run 2’. In: *Eur. Phys. J. C* 80.1 (2020), p. 47. DOI: 10.1140/epjc/s10052-019-7500-2. arXiv: 1909.00761 [hep-ex]. №: CERN-EP-2019-169.
- [29] *LHCb.* ‘A comprehensive real-time analysis model at the LHCb experiment’. In: *JINST* 14.04 (2019), P04006. DOI: 10.1088/1748-0221/14/04/P04006. arXiv: 1903.01360 [hep-ex]. №: CERN-LHCb-DP-2019-002.
- [30] *CMS.* ‘Search for narrow resonances in dijet final states at $\sqrt{s} = 8\text{ TeV}$ with the novel CMS technique of data scouting’. In: *Phys. Rev. Lett.* 117.3 (2016), p. 031802. DOI: 10.1103/PhysRevLett.117.031802. arXiv: 1604.08907 [hep-ex]. №: CMS-EXO-14-005 and CERN-EP-2016-090.

- [31] *CMS*. ‘Search for a Narrow Resonance Lighter than 200 GeV Decaying to a Pair of Muons in Proton-Proton Collisions at $\sqrt{s} = 13$ TeV’. In: *Phys. Rev. Lett.* 124.13 (2020), p. 131802. DOI: 10.1103/PhysRevLett.124.131802. arXiv: 1912.04776 [hep-ex]. №: CMS-EXO-19-018 and CERN-EP-2019-265.
- [32] *CMS*. ‘Search for long-lived particles decaying into muon pairs in proton-proton collisions at $\sqrt{s} = 13$ TeV collected with a dedicated high-rate data stream’. In: *JHEP* 04 (2022), p. 062. DOI: 10.1007/JHEP04(2022)062. arXiv: 2112.13769 [hep-ex]. №: CMS-EXO-20-014 and CERN-EP-2021-266.
- [33] *CMS*. ‘Recording and reconstructing 10 billion unbiased b hadron decays in CMS’ (Oct. 2019). URL: cds.cern.ch/record/2704495. №: CMS-DP-2019-043.
- [34] Z. Citron et al. ‘Report from Working Group 5: Future physics opportunities for high-density QCD at the LHC with heavy-ion and proton beams’. *Report on the Physics at the HL-LHC, and Perspectives for the HE-LHC*. Ed. by A. Dainese, M. Mangano, A. B. Meyer, A. Nisati, G. Salam, and M. A. Vesterinen. Vol. 7. Dec. 2019, pp. 1159–1410. DOI: 10.23731/CYRM-2019-007.1159. arXiv: 1812.06772 [hep-ph]. №: CERN-LPCC-2018-07.
- [35] R. Bruce et al. *HL-LHC operational scenario for PbPb and pPb operation*. Tech. rep. CERN-ACC-2020-0011. 2020. URL: cds.cern.ch/record/2722753.
- [36] R. Bruce et al. ‘New physics searches with heavy-ion collisions at the CERN Large Hadron Collider’. In: *J. Phys. G* 47.6 (2020), p. 60501. DOI: 10.1088/1361-6471/ab7ff7. arXiv: 1812.07688 [hep-ph].
- [37] D. d’Enterria et al. ‘Opportunities for new physics searches with heavy ions at colliders’. *2022 Snowmass Summer Study*. Mar. 2022. arXiv: 2203.05939 [hep-ph].
- [38] Y. D. He. ‘Search for a Dirac magnetic monopole in high-energy nucleus-nucleus collisions’. In: *Phys. Rev. Lett.* 79 (1997), p. 3134. DOI: 10.1103/PhysRevLett.79.3134.
- [39] O. Gould and A. Rajantie. ‘Magnetic monopole mass bounds from heavy ion collisions and neutron stars’. In: *Phys. Rev. Lett.* 119 (2017), p. 241601. DOI: 10.1103/PhysRevLett.119.241601. arXiv: 1705.07052 [hep-ph]. №: IMPERIAL-TP-2017-OG-2.
- [40] O. Gould, D. L.-J. Ho, and A. Rajantie. ‘Towards Schwinger production of magnetic monopoles in heavy-ion collisions’. In: *Phys. Rev. D* 100 (2019), p. 015041. DOI: 10.1103/PhysRevD.100.015041. arXiv: 1902.04388 [hep-th]. №: IMPERIAL-TP-2019-DH-01 and HIP-2019-2/TH.
- [41] *MoEDAL*. ‘Search for magnetic monopoles produced via the Schwinger mechanism’. In: *Nature* 602.7895 (2022), p. 63. DOI: 10.1038/s41586-021-04298-1. arXiv: 2106.11933 [hep-ex].
- [42] S. Knapen, T. Lin, H. K. Lou, and T. Melia. ‘Searching for Axionlike Particles with Ultraperipheral Heavy-Ion Collisions’. In: *Phys. Rev. Lett.* 118.17 (2017), p. 171801. DOI: 10.1103/PhysRevLett.118.171801. arXiv: 1607.06083 [hep-ph].
- [43] *CMS*. ‘Evidence for light-by-light scattering and searches for axion-like particles in ultraperipheral PbPb collisions at $\sqrt{s_{NN}} = 5.02$ TeV’. In: *Phys. Lett. B* 797 (2019), p. 134826. DOI: 10.1016/j.physletb.2019.134826. arXiv: 1810.04602 [hep-ex]. №: CMS-FSQ-16-012 and CERN-EP-2018-271.
- [44] *ATLAS*. ‘Measurement of light-by-light scattering and search for axion-like particles with 2.2 nb⁻¹ of PbPb data with the ATLAS detector’. In: *JHEP* 11 (2021), p. 50. DOI: 10.1007/JHEP11(2021)050. arXiv: 2008.05355 [hep-ex]. №: CERN-EP-2020-135.

- [45] M. Drewes, A. Giammanco, J. Hajer, and M. Lucente. ‘New long-lived particle searches in heavy-ion collisions at the LHC’. In: *Phys. Rev. D* 101.5 (2020), p. 55002. DOI: 10.1103/PhysRevD.101.055002. arXiv: 1905.09828 [hep-ph]. №: CP3-19-26.
- [46] B. Batell, T. Ghosh, and K. Xie. ‘Heavy Neutral Lepton Searches at the Electron-Ion Collider: A Snowmass Whitepaper’. Mar. 2022. arXiv: 2203.06705 [hep-ph]. №: PITT-PACC-2206.
- [47] V. Goncalves and B. Moreira. ‘Dark photons from pions produced in ultraperipheral PbPb collisions’. In: *Phys. Lett. B* 808 (2020), p. 135635. DOI: 10.1016/j.physletb.2020.135635. arXiv: 2006.08348 [hep-ph].
- [48] A. L. S. Angelis, E. Gladysz-Dziadus, Y. V. Kharlov, V. L. Korotkikh, G. Mavromanolakis, A. D. Panagiotou, and S. A. Sadovsky. ‘Model of Centauro and strangelet production in heavy ion collisions’. In: *Phys. Atom. Nucl.* 67 (2004). [*Yad. Fiz.* 67, 414 (2004)], p. 396. DOI: 10.1134/1.1648929. arXiv: nucl-th/0301003 [nucl-th]. №: IHEP-2002-8.
- [49] *STAR*. ‘Strangelet search at RHIC’. In: *Phys. Rev. C* 76 (2007), p. 011901. DOI: 10.1103/PhysRevC.76.011901. arXiv: nucl-ex/0511047 [nucl-ex].
- [50] D. L.-J. Ho and A. Rajantie. ‘Electroweak sphaleron in a strong magnetic field’. In: *Phys. Rev. D* 102 (2020), p. 053002. DOI: 10.1103/PhysRevD.102.053002. arXiv: 2005.03125 [hep-th]. №: IMPERIAL-TP-2020-DH-01.
- [51] L. Beresford and J. Liu. ‘New physics and tau $g - 2$ using LHC heavy ion collisions’. In: *Phys. Rev. D* 102.11 (2020), p. 113008. DOI: 10.1103/PhysRevD.102.113008. arXiv: 1908.05180 [hep-ph].
- [52] M. Dyndal, M. Klusek-Gawenda, M. Schott, and A. Szczurek. ‘Anomalous electromagnetic moments of τ lepton in $\gamma\gamma \rightarrow \tau^+\tau^-$ reaction in PbPb collisions at the LHC’. In: *Phys. Lett. B* 809 (2020), p. 135682. DOI: 10.1016/j.physletb.2020.135682. arXiv: 2002.05503 [hep-ph].
- [53] *CMS*. ‘Measurement of B_s^0 meson production in pp and PbPb collisions at $\sqrt{s_{NN}} = 5.02$ TeV’. In: *Phys. Lett. B* 796 (2019), pp. 168–190. DOI: 10.1016/j.physletb.2019.07.014. arXiv: 1810.03022 [hep-ex]. №: CMS-HIN-17-008 and CERN-EP-2018-257.
- [54] *CMS*. ‘Observation of the B_c^+ Meson in PbPb and pp Collisions at $\sqrt{s_{NN}} = 5.02$ TeV and Measurement of its Nuclear Modification Factor’. In: *Phys. Rev. Lett.* 128.25 (2022), p. 252301. DOI: 10.1103/PhysRevLett.128.252301. arXiv: 2201.02659 [hep-ex]. №: CMS-HIN-20-004 and CERN-EP-2021-259.
- [55] R. Bruce et al. ‘Plans for LHC ion operation in Run 3’. *10th LHC Operations Workshop*. CERN. Geneva, Switzerland, Nov. 2021. URL: indico.cern.ch/event/1077835/contributions/4533358.
- [56] J. Alwall et al. ‘The automated computation of tree-level and next-to-leading order differential cross sections, and their matching to parton shower simulations’. In: *JHEP* 7 (2014), p. 79. DOI: 10.1007/JHEP07(2014)079. arXiv: 1405.0301 [hep-ph]. №: CERN-PH-TH-2014-064, CP3-14-18, LPN14-066, MCNET-14-09, and ZU-TH-14-14. Code: *MadGraph5_aMC@NLO: A Monte Carlo at next-to-leading order*. Jan. 1994. GitHub: [mg5amcnlo/mg5amcnlo](https://github.com/mg5amcnlo/mg5amcnlo). URL: madgraph.phys.ucl.ac.be.
- [57] A. Buckley et al. ‘LHAPDF 6: Parton density access in the LHC precision era’. In: *Eur. Phys. J. C* 75 (2015), p. 132. DOI: 10.1140/epjc/s10052-015-3318-8. arXiv: 1412.7420 [hep-ph]. №: GLAS-PPE-2014-05, MCNET-14-29, IPPP-14-111, and DCPT-14-222.

- [58] R. D. Ball et al. ‘Parton distributions with LHC data’. In: *Nucl. Phys. B* 867 (2013), pp. 244–289. DOI: 10.1016/j.nuclphysb.2012.10.003. arXiv: 1207.1303 [hep-ph]. №: EDINBURGH-2012-08, IFUM-FT-997, FR-PHENO-2012-014, RWTH-TTK-12-25, CERN-PH-TH-2012-037, and SFB-CPP-12-47.
- [59] S. Dulat et al. ‘New parton distribution functions from a global analysis of quantum chromodynamics’. In: *Phys. Rev. D* 93.3 (2016), p. 033006. DOI: 10.1103/PhysRevD.93.033006. arXiv: 1506.07443 [hep-ph].
- [60] K. J. Eskola, P. Paakkinen, H. Paukkunen, and C. A. Salgado. ‘EPPS 16: Nuclear parton distributions with LHC data’. In: *Eur. Phys. J. C* 77.3 (2017), p. 163. DOI: 10.1140/epjc/s10052-017-4725-9. arXiv: 1612.05741 [hep-ph].
- [61] C. Bierlich et al. ‘A comprehensive guide to the physics and usage of PYTHIA 8.3’ (Mar. 2022). arXiv: 2203.11601 [hep-ph]. №: LU-TP 22-16, MCNET-22-04, and FERMILAB-PUB-22-227-SCD. Code: *Pythia: The Lund Monte Carlo event generator for high- p_T physics*. Feb. 1983. URL: `pythia.org`.
- [62] Y. Gershtein and S. Knapen. ‘Trigger strategy for displaced muon pairs following the CMS phase II upgrades’. In: *Phys. Rev. D* 101.3 (2020), p. 32003. DOI: 10.1103/PhysRevD.101.032003. arXiv: 1907.00007 [hep-ex].
- [63] Bierlich, Christian and Gustafson, Gösta and Lönnblad, Leif and Shah, Harsh. ‘The Angantyr model for Heavy-Ion Collisions in PYTHIA 8’. In: *JHEP* 10 (2018), p. 134. DOI: 10.1007/JHEP10(2018)134. arXiv: 1806.10820 [hep-ph]. №: LU-TP-18-19, LU-TP 18-19, and MCNET-18-12.
- [64] P. Skands, S. Carrazza, and J. Rojo. ‘Tuning PYTHIA 8.1: the Monash 2013 Tune’. In: *Eur. Phys. J. C* 74.8 (2014), p. 3024. DOI: 10.1140/epjc/s10052-014-3024-y. arXiv: 1404.5630 [hep-ph]. №: CERN-PH-TH-2014-069, MCNET-14-08, and OUTP-14-05P.
- [65] *ATLAS*. ‘The Pythia 8 A3 tune description of ATLAS minimum bias and inelastic measurements incorporating the Donnachie-Landshoff diffractive model’ (Aug. 2016). №: ATL-PHYS-PUB-2016-017.